Constitutive modelling of deformation behavior of glassy polymers and applications

Tomita, Yoshihiro

(Citation)
International Journal of Mechanical Sciences,42(8):1455-1469

(Issue Date)
2000

(Resource Type)
journal article

(Version)
Accepted Manuscript

(URL)
https://hdl.handle.net/20.500.14094/90000034

Constitutive Modelling of Deformation Behavior of Glassy Polymers and Applications

Yoshihiro Tomita
Faculty of Engineering, Kobe University
Nada, Kobe, Japan 657-8501

Abstract

The purpose of the present article is to provide a perspective of constitutive equations for glassy polymers developed using the molecular chain network theory. The results of experimental observations of the deformation behavior of glassy polymers at macro- and micro-scale are indicated, and an accommodation of the characteristic feature of deformation behavior into the molecular chain network theories is discussed. The related computational simulations of neck formation and its propagation under plane strain and three dimensional conditions are illustrated. The results clarified the three dimensional characteristic feature of neck propagation behavior under isothermal condition and the effect of deformation induced heat and pre-drawing on the plane strain neck propagation behavior.

Keywords: Glassy polymer, Constitutive equation, Network models, Nonaffine model, Computational simulation, Neck propagation, Thermomechanical coupling, Predrawing, AFM observation

Dr. Yoshihiro TOMITA
Professor
Department of Mechanical Engineering
Faculty of Engineering, Kobe University
Nada, Kobe, 657-8501 JAPAN
Tel: +81-78-803-1110 Fax: +81-78-803-1131
tomita@mech.kobe-u.ac.jp http://solid.mech.kobe-u.ac.jp

1. Introduction

The deformation behavior of polymeric materials under tension is very different from that of metallic materials. The necking instability develops in a specimen and subsequently propagates along the tensile direction under essentially steady-state conditions. The characteristic hardening observed in the necking region is generally caused by the alignment of molecular chains which were randomly oriented in the undeformed state, and is responsible for the development of necking and its propagation.

In order to reproduce the characteristic feature of the deformation behavior, James and Guth [1] developed a model that accounts for the evolution of the microstructure of the glassy polymer. Subsequently, a general three-dimensional constitutive model was established based on the three-chain model [2] using the generalized Argon double-kink model [3]. Further generalization of the model to the eight-chain model [4] and the full network model [5] has been done. In these models, the polymeric material is approximated by a molecular chain network system defined by the cross-links, which are assumed to be physically entangled points of molecular chains, whose numbers remain constant during the deformation. Therefore, these models are referred to as the affine model. The constitutive equation obtained can well reproduce the tension and compression behaviors, whereas, the shear strength is likely to overestimate [5]. This is partially attributable to the change in the number of entangled points due to the difference in the development of internal microstructures, depending on the local deformation. Indeed, the results of experimental investigations implicitly suggest the possibility of a change in configuration of the entangled points due to deformation and a change in temperature [6,7], which causes a change in the rigidity of the polymeric materials. Tomita and co-workers [8,9] proposed the nonaffine model based on the molecular chain network theory, in which a change of the number of entangled points was taken into account. Furthermore, based on the atomic force microscope (AFM) observation of the surface of the polycarbonate (PC), micro- to macroscopic transition of the deformation and the problems associated with the framework of the constitutive equation related to the associativeness of the direction of principal plastic stretch to that of the alignment of molecular chains have been discussed [10,11].

In this paper, the characteristic deformation behaviors of glassy polymers are depicted from an experimental observation and the constitutive equations, based on the molecular chain network theory which can accommodate the experimentally observed features, are discussed. The computational predictions of the necking behavior in polymeric materials deformed under different conditions will be clarified.

2. Constitutive Equations

2.1 Experimental Observation of Deformation Behaviors of Glassy Polymer

Figures 1(b) and (c) indicate the typical nominal stress vs elongation relation with the deformed profile of the PC specimen shown in Fig.1 (a) and the true stress versus logarithmic strain relation for PC under tension, respectively. The necking instability develops in a specimen and subsequently propagates along the tensile direction under essentially steady-state conditions. The initial isotropy of the materials was confirmed through the tension test of specially prepared specimens with different direction angles with respect to original PC block. Similar phenomena can be seen in simple shear deformation of the specimen where the shear band formation and propagation along the direction perpendicular to the shear direction were reported [12]. Although, different types of instabilities are involved, their propagation are generally explained by substantial hardening in the later stage of deformation, as depicted in Fig.1(c), caused by the alignment of molecular chains which were randomly oriented in the undeformed state.

However, the relationship between the micro- and macroscopic behaviors of polymeric materials, that has a hierarchical structure at successive molecular to macrolevels, has not yet been fully clarified. The recent investigation partially clarified the micro- to macroscopic transition of the deformation through the Atomic Force Microscope (AFM) observation of the surface of PC. Figure 2 indicates the typical surface structural change in the PC specimen during the deformation [10, 11]. In the insert in Fig. 2, a to e indicate the locations of the target points and ξ, η is the coordinate with the origin at the necking center. At a, the initially very flat surface starts to undulate and a microfibril bundle structure is formed along the tensile direction. During neck formation and propagation c, a similar microfibril structure with shorter wavelength appears. At e, representing the after neck propagation state, a further subdivision of the waves was observed as the deformation progressed. Subsequently, a thin microfibril structure with a short wavelength remains as a permanent deformation. The misalignment between the tensile direction and the direction of the microfibril can be observed. Figure 3 shows the direction of plastic stretch θ_p which was estimated by measuring the average deformation over a $20\mu m$ square region marked on the surface of the specimen and that of aligned microfibril structures θ_f which was determined from the maximum spectrum of the two-dimensional Fourier transformation of the AFM image [11]. ε_{xy} indicates the shear strain measured in the same way as for θ_p. Standard deviation from measuring number n is also indicated. In the figure, W_0 to W_5 indicate the lines initially parallel to the tension direction y from the center of the specimen to the side edge. Although, the amount is rather small, due to the increase of the shear strain caused by the propagation of the neck, the aligned direction of the microfibril tends to

separate from the principal plastic stretch direction. This implies that the rotation of microfibril, which is a bundle of molecular chains, lags behind that of the principal direction of plastic stretch due to shear strain.

2.2 Formulation of Constitutive Equations

To duplicate the experimentally observed characteristic feature of the glassy polymers, in the molecular chain network model, as shown in Fig.4, the microstructure of a glassy polymer is assumed to consist of long molecular chains which are randomly distributed in space. A single chain, which consists of several segments containing monomers, is defined by the two cross-links which are assumed to be physically entangled points of molecular chains and their numbers are assumed to remain constant during deformation. These results in a networklike structure as in rubber, but with the chemical cross-links replaced by physical entanglements. According to the theory of Harward and Thackray [13], the glassy polymer must overcome two physically distinct sources of resistance before large strain inelastic flow may occur. Below the glass transition temperature, prior to the initial yield, the material must be stressed to exceed its intermolecular resistance to segment rotation. Once the material is free to flow, molecular alignment occurs and results in an anisotropic internal resistance to further inelastic deformation, which is referred to as orientation hardening.

The intermolecular resistance to plastic flow is considered to be due to the impedance imposed by neighboring chains on the ability of a chain segment to rotate. Based on the assumption that plastic flow occurs due to double kinking of molecular chains, Argon [3] developed the constitutive equation for the plastic shear strain rate, $\dot{\gamma}^p$:

$$\dot{\gamma}^p = \dot{\gamma}_0 \exp\left[\left(-As_0/T\right)\left\{1-\left(\tau/s_0\right)^{5/6}\right\}\right] \tag{1}$$

where $\dot{\gamma}_0$ and A are constants, T is the absolute temperature, $s_0 = 0.077G/(1-\nu)$ is the athermal shear strength, G is the elastic shear modulus, ν is Poisson's ratio and τ is the applied shear stress. Boyce et al. [2] extended this expression to include the effect of pressure. They used $s + ap$ instead of s_0, where s is the shear strength which changes with the plastic strain from s_0 to a stable value s_{ss}, p is the pressure and a is a pressure-dependent coefficient. Since s depends on temperature and strain rate, the evolution equation of s can be expressed as $\dot{s} = h\left\{1-\left(s/s_{ss}\right)\right\}\dot{\gamma}^p$ where h is the rate of resistance with respect to plastic strain.

When a polymeric material experiences a stress that exceeds its intermolecular resistance, molecular chain alignment occurs. This alignment generates back-stress. The initial structure of the molecular chain network is assumed to be isotropic. After yielding, the molecular chains are stretched and tend to align along the principal direction of plastic

stretch, which reduces the configuration entropy of the molecular chain network system and therefore increases the internal resistance for further deformation. This internal resistance can be expressed as a back-stress using the molecular chain network theory. As indicated by the AFM observation of the surface of PC [10,11], the coaxiality of the principal stretch direction and the direction of the molecular chain is not necessarily satisfied by increasing the shear deformation with material rotation. However, the amount of noncoaxiality is rather small so that the principal component of back-stress is taken to be coaxial with the left plastic stretch tensor in the first approximation. In such a case, the principal components of the back-stress tensor for the eight-chain model [4], which is widely used in computational simulations, can be employed as

$$
\begin{aligned}
&B_i = \frac{1}{3} C^R \sqrt{N} \frac{V_i^2 - \lambda^2}{\lambda} L^{-1}\left(\frac{\lambda}{\sqrt{N}}\right) \\
&L(x) = \coth x - 1/x \\
&\lambda^2 = \frac{1}{3}(V_1^2 + V_2^2 + V_3^2)
\end{aligned}
\tag{2}
$$

where B_i is the principal component of back-stress, V_i is the principal plastic stretch, $\lambda_L = \sqrt{N}$ is the locking stretch, i.e., limiting stretch in tension, N is the average number of segments in a single chain, $C^R = nkT$ is a constant, n is the number of chains per unit volume, k is Boltzmann's constant, and L is the Langevin function. In the eight-chain model [4] and the other models [2],[5], the entangled points of molecular chains are assumed to be fixed during the deformation, and the average number of segments, N, is constant. Therefore, these models are referred to as the affine models. However, it has been clarified that the deformation behavior under compression and tension can be well predicted using affine models, whereas the shear strength is likely to be overestimated [5]. This is partially attributable to the change in the number of entangled points due to the difference in the development of internal microstructures, depending on the local deformation. An increase in the number of entangled points reduces the average number of segments in polymeric chains, which causes a reduction in the extendibility and an increase in the relative stiffening of the materials. A decrease in the number of entangled points cause an opposite effect. Experimental observations implicitly suggest the possibility of a change in the configuration of the entangled points due to deformation and change in temperature [6,7].

To accommodate the change in the entangled situation due to the deformation and the temperature change, Tomita and coworkers [8,9] proposed a nonaffine model in which the change in the number of entangled points was taken into account. Tomita and Adachi [14] gave the simplest form of the number of entangled points m expressed as function of the temperature T and the variable ξ representing the local deformation of polymeric material.

$$m(T,\xi) = m_0[1 + d\{\exp(-E_a / RT_0) - \exp(-E_a / RT)\}]\{-c(1-\xi)\} \qquad (3)$$

m_0 Are the number of entangled points at the reference temperature $T = T_0$ and the initial state of deformation $\xi = 1$. The variable ξ that reflects the change in the relative angle of the coordinate axes with unit base vectors g_i which are embedded parallel to the directions of principal plastic stretch in the initial stage of plastic deformation and deform into G_i with the subsequent deformation. For volume-constant deformation $\xi = 1/(|G_1||G_2||G_3|)$. c and d are the material constants and E_a and R are the dissociation energy and the universal gas constant, respectively. The decrease in ξ and an increase in the temperature T causes the reduction of the number of entangled points m. Correspondingly, the average number of segments in a single chain increases, which results in the additional extendibility of the materials.

The deformation gradient F from the initially isotropic state of the polymeric material can be decomposed into the elastic part F^e and plastic part F^p. F^p represents the relaxed configuration obtained by unloading without rotation and permanent orientation of molecular alignment. The magnitude of the plastic deformation rate tensor d^p is assumed to be given by the representative plastic shear strain rate $\dot{\gamma}^p$, and the direction is specified by the normalized deviatoric part of the driving stress $\tilde{\sigma}'$ [2]. Then

$$\begin{aligned} d^p &= \dot{\gamma}^p \tilde{\sigma}' / \sqrt{2}\tau \\ \tilde{\sigma} &= \sigma - F^e B F^{e-1} / \det F^e \\ \tau &= \left(\tilde{\sigma}'\tilde{\sigma}' / 2\right)^{1/2}, \end{aligned} \qquad (4)$$

where σ is the Cauchy stress tensor and B is the back-stress tensor with principal values B_i in Eq.(2). The shear stress τ in Eq.(1) is estimated by Eq.(4). The complete elastoplastic constitutive equation can be established by introducing the thermoelastic constitutive equation for the elastic part of the deformation rate tensor.

The material parameters for the eight-chain model used by Wu and Van der Giessen [5] are employed for the affine model for PC. The newly introduced material parameters c and d in Eq.(3) are determined from experimental results for shear deformation under isothermal conditions obtained by G'Sell and Gopez [12] and for tension under different environmental temperatures with a low strain rate [15]. Thus obtained material parameters, $E / s_0 = 23.7$, $s_{ss} / s_0 = 0.79$, $h / s_0 = 5.15$, $As_0 / T_0 = 78.6$, $\alpha = 0.08$, $\dot{\gamma}_0 = 2.0 \times 10^{15} / s$, $s_0 = 97\,MPa$, $T_0 = 296K$, $m_0 = 7.83 \times 10^{26}$, $d = 214$ and $c = 0.33$ provide the complete set of material parameters.

3. Governing Equation

In this section, the governing equations for an elastoplastic boundary value problem are given within the context of large-strain theory. An updated Lagrangian formulation of the field and constitutive equations are employed. Consider an equilibrium state for a body with volume V and surface S subjected to a constraint velocity on S_v and given traction on S_t. Each particle is labeled by a set of curvilinear coordinate x^i which are embedded in the body in the current state and serve as independent variables. In the deformed body the covariant components of the metric tensor are denoted by G_{ij}. The weak form of the equation governing the rates of stress and traction yields the virtual work principle [16,17]

$$\int_V (\dot{S}^{ji} + \sigma^{lj} V^i{}_{;l}) \delta V_{i:j} dV = \int_{S_t} \dot{P}_i \delta V_i dS \tag{5}$$

where $\dot{P}_i$ is the nominal traction rate and δV_i is the virtual velocity satisfying the homogeneous boundary conditions over surface S_v. S^{ij} is the Kirchhoff stress tensor, which is identical to the Cauchy stress tensor σ^{ij} in the current configuration. The overdot denotes the material time derivative with respect to current coordinates and $(\ )_{;l}$ denotes the covariant derivative with respect to current coordinates.

The weak form of the energy balance equation for the same body subjected to prescribed heat flux $Q = -n_i q^i$ on S_q with the surface unit normal n_i and constraint temperature on S_T can be expressed as [16,17]

$$\int_V \delta T \rho c \dot{T} dV + \int_V \delta T_{,i} \kappa^{ij} T_{,j} dV = \int_V \delta T \chi \dot{w}^p dV + \int_{S_q} \delta T Q dS \tag{6}$$

where ρ, c and κ^{ij} are the mass density, specific heat capacity and the thermal conductivity tensor, respectively. $(\ )_{,i}$ denotes the partial derivative with respect to current coordinates. The fraction χ of irreversible work, $\dot{w}^p = \sigma^{ij} \dot{\varepsilon}^p_{ij}$ is converted to heat. The specific form of heat flux Q on S_q depends on the respective boundary conditions.

4. Computational Prediction of Instability Propagation

In this section, two- and three- dimensional neck propagations under isothermal and thermomechanically coupled conditions will be discussed. The numerical procedure employs the finite-element methods established based on the virtual work principle Eq. (5) along with the proposed constitutive equation. Meanwhile, the finite-element differential heat

conduction equation established by the weak form expression of the energy balance equation (6) in conjunction with Fourier's law of heat conduction [18,19] was employed. The Houbolt method [18] is used here to transform the differential equation into a finite-difference equation in the time domain. These two finite-element equations in space were solved simultaneously for the thermomechanical coupling problems. With regard to the value of the fraction of heat dissipated χ, the precise discussion has not been given for the polymeric materials so that we expected that $\chi = 0.95$ as employed in our researchs [14],[19].

4.1 Three-dimensional neck propagation under isothermal conditions

To clarify the three-dimensional neck propagation behavior under isothermal conditions, the computational model of a specimen subjected to uniform tension at both ends under shear-free conditions, as shown in Fig. 5(b), is employed. In order to initiate necking at the center of the specimen, an initial geometrical imperfection of the width is introduced. Due to the symmetry of the deformation, the finite element discretization with quadratic block elements shown in Fig.5 (b) is employed for 1/8 of the specimen, as shown in the figure. The computation was performed with $\dot{u} / L_0 = 4 \times 10^{-4} / s$ and the same material parameters as indicated in section 2.

Figure 6 (a) shows the nominal stress σ_n / s_0, and the lateral contraction ratios $1 - H / H_0$ and $1 - t / t_0$ with respect to width and thickness, respectively, at cross sections AA and BB shown in Fig. 5 (b) vs elongation u / L_0. The nominal stress increases proportionally with strain and attains the maximum when necking starts, then stress drops to the local minimum values with neck development at the fixed point. With further deformation, hardening due to orientation of molecular chains, which starts at the neck, causes the unnecked part to start neck propagation along the tensile direction with approximately constant stress. Finally, the maximum stretch approaches the locking stretch λ_L, beyond which the stress starts to increase again [20]. The lateral contraction in cross section AA starts with the onset of necking and then stabilizes as neck propagates along the specimen. On the other hand, at cross section BB, lateral contraction is small during neck propagation but rapidly increase as the neck arrives, and attains the secondary steady state.

Figure 6(b) shows the specimen profiles and representative strain rate $\dot{\varepsilon}^p / \dot{\varepsilon}_0$ distributions at a to f as indicated in Fig.6(a). The representative strain rate distributions clearly indicate the three-dimensional neck propagation behavior. Necking starts and progresses in the vicinity of the center of the specimen with strain. The neck propagation is visible over $u / L_0 = 0.1$ to 0.5, where, as shown in Fig. 6 (a) the stress is approximately constant. The maximum-strain-rate region in the plane with $x_1 = 0$ precedes that of the plane with $x_1 = H_0$ in the undeformed state. This is partially attributable to the constraint of the deformation in the width direction. A similar neck propagation behavior observed in the plane with $x_1 = 0$ can be seen in the results of plane strain blocks obeying the constitutive

equation derived by the affine model [21]. The representative strain rate distributions confirm the three dimensionality of the strain distribution, which indicates the difficulty of determining material parameters through simple experimentation alone. The related research was published in [20].

4.2 Thermomechanically coupled neck propagation behavior under plane strain condition

In order to clarify the thermomechanically coupled deformation behavior, tension of the blocks deformed under the plane strain condition have been simulated using the same material parameters as in section 2 and the computational model as shown in Fig. 5(a). Uniform temperature distribution with $T = T_0$ is initially assumed throughout the block, and the heat generated by irreversible work is assumed to be discharged through convection to the air at the side surface. The remaining surfaces are assumed to be adiabatic boundaries. To avoid the extreme softening due to temperature rise, the simulation was stopped when the number of entangled points decreased to 40% of the initial number m_0.

Figure 7(a) shows the overall deformation behaviors such as the nominal stress σ_n / s_0 applied and the contraction of cross-section v / W_0 versus elongation u / L_0. Fig. 7 (b) shows the deformed specimen profiles, and the distributions of representative strain rate $\dot{\varepsilon}^p / \dot{\varepsilon}_0$, change of temperature $\Delta T / T_0$, distortion ξ and the change in the number of entangled points $\Delta m / m_0$ for $u / L_0 = 0.4$. For $\dot{U} = 10^4$, the results correspond to those for $u / L_0 = 0.18$ where the simulation was stopped due to the superfluous reduction of the number of entangled points. Except for the case of $\dot{U} = 10^4$, the average stress attains the maximum and subsequently drops to the local minimum with necking, and almost steady-state deformation that preserves the constant applied force arises. For the case of $\dot{U} = 1$, virtually isothermal conditions are achieved, as observed in Fig. 7(b), and the maximum stretch approaches the locking stretch in the early stage of deformation, so that the average stress starts to increase again in the later stage of deformation. For the case of $\dot{U} = 10^2$, the additional increase in locking stretch is caused by the dissociation of entangled points due to a temperature rise, as shown in Fig.7(b), so that the steady-state region lasts longer. However, a softening caused by surplus dissociation of entangled points results in necking without propagation, as in the case of $\dot{U} = 10^4$. From v / W_0 and the corresponding neck profile, we can see that with an increase in the end velocity, the neck becomes larger and more localized. The typical local deformation behavior is seen in the case of $\dot{U} = 10^2$. Due to the convection of the heat produced by irreversible work from the side surface to the air, the highest- temperature region is located at the center of the specimen and it propagates with some amount of delay corresponding to the heat conduction time. On the other hand, although the change in the values of distortion ξ is rather small, it is affected by the profile of the neck, e.g., the deformation of the polymeric material. The maximum reduction of ξ is observed at the shoulder of the neck where large distortion of the material occurs, and the

rate of change of ξ decreases as the location moves into the interior of the specimen, which is attributable to the increase in the symmetry of deformation. Thus, the temperature and distortion contribute to the reduction of the number of entangled points at different parts of the specimen; however, under the present deformation conditions, the number of entangled points is strongly affected by the change of temperature, such that the distribution in the number of entangled points becomes similar to that of temperature. In the case of the high strain rate $\dot{U} = 10^4$, both temperature and distortion contribute to the reduction in the number of entangled points, i.e., softening, at the same part of the specimen, as can be seen in Fig.7(b), which results in neck formation without propagation.

4.3 Neck propagation behavior with predrawing

A polymeric material with predrawing exhibits anisotropy depending on the deformation, due to orientation of molecular chains. Correspondingly, predrawing may affect the neck and shear band propagation behavior. Here, the computational prediction of the predrawing-induced anisotropic behavior of a polymeric material is discussed.

Figure 5(a) indicates the computational model for plane strain blocks with predrawing defined by the predraw ratio PDR and predraw direction θ with respect to tensile direction, subjected to uniform tension at both ends under a shear-free condition. The material parameters used are the same as those in section 2. The computation was performed under the environmental temperature of $T_0 = 296K$ and a nominal end velocity of $\dot{\varepsilon}_0 = \dot{u} / L = 0.01 / s$.

Figure 8(a) shows the nominal stress, σ_n / s_0, vs elongation, u / L, for the blocks with $PDR = 1.4$ and $\theta = 0 - 90^\circ$. Regardless the pre-drawing direction, a decrease in the force due to the onset of necking and subsequent stationalization of the stress due to the neck propagation can be observed. Increase in the angle θ causes a decrease in nominal stress and a delay in the neck propagation. These are the characteristic feature of anisotropic response caused by predrawing.

In order to clarify the neck propagation process in the blocks with different θ and λ_0, the distribution of the representative strain rate, $\dot{\varepsilon}^p / \dot{\varepsilon}_0$, for $u / L = 0.05, 0.15$ is shown in Fig. 8(b). In the early stage of deformation, $u / L = 0.05$, two intersecting shear bands are observed. The predominant shear band is parallel to the predrawing direction, and remains predominant during the deformation process. This tendency coincides with the experimental observation [2]. Further comparison clarifies that the shear band developed near the center of the specimen propagates towards the two ends accompanied by necking.

6. Concluding Remarks

A perspective has been given on the constitutive equations based on molecular

chain network models which are indispensable for the precise prediction of deformation behavior, and a critical discussion associated with their applicability has been given. The topics were selected from three dimensional and plane strain thermocoupled neck propagation behavior.

Computational predictions of instability behavior can play a very important role in the understanding and modeling of the wide range of deformation behavior of polymeric materials, and will contribute to improving the fabrication processes of the thin films and fibers. Further research clarifying the continuous transition from micro- to macroscopic deformation behavior, the development of direct physical approaches for each class and bridging of the substantial size and time gaps between the different classes are essential in order to produce functional materials created by strain-induced orientation of molecular chains. The related research based on molecular dynamics theory and SEM and AFM observations are expected to solve the related problems, and intensive studies are now under way.

Acknowledgments

Financial support from the Ministry of Education of Japan and Kawanishi Foundation is gratefully acknowledged. I wish to thank Idemitsu Kosan Ltd. for providing the materials and unpublished data, Dr. T. Adachi for the valuable discussion and the graduate student Mr. S. Tanaka for the assistance with the calculations.

References

1. James, H. M. and Guth, E., Theory of the elastic properties of rubber. J. Chem. Phys. 1943, **11**, 455-481.

2. Boyce, M. C., Parks, D. M. and Argon, A. S., Large inelastic deformation of glassy polymers, Part I: rate dependent constitutive model. Mech. Mater., 1988. **7,**15-33.

3. Argon, A. S., A theory for the low-temperature plastic deformation of glassy polymers. Phil. Mag. 1973, **28**,839-865.

4. Arruda, E. M. and Boyce, M. C., A three-dimensional constitutive model for large stretch behavior of rubber materials. J. Mech. Phys. Solids, 1993, **41**,389-412.

5. Wu, P. D. and Van der Giessen, E., On improved network models for rubber elasticity and their applications to orientation hardening in glassy polymers. J. Mech. Phys. Solids, 1993, **41**,427-456.

6. Raha, S. and Bowden, P. B., Birefringence of plastically deformed poly (methyl methacrylate). Polymer, 1972, **13**,174-183.

7. Botto, P. A., Duckett, R. A. and Ward, I. M., The yield and thermoelastic properties of oriented poly (methyl methacrylate). Polymer , 1987, **28**, 257-262.
8. Tomita, Y. and Tanaka, S., Prediction of deformation behavior of glassy polymers based on molecular chain network model. Int. J. Solids Structures, 1995, **32**, 3423-3434.
9. Tomita, Y., Adachi, T., and Tanaka, S., Modelling and Aplication of Constitutive Equation for Glassy Polymer Based on Nonaffine Network Theory. Eur. J. Mech. A/Solids, ,1997, **16**, 745-755.
10.Kashu,Y., Adachi, T. and Tomita, Y., AFM observation of microscopic behavior of glassy polymer with application to understanding of macroscopic behavior. Eds. Abe, T and Tsuta, T, Proc. AEPA'96 Pergamon, 1996, 501-505.
11.Adachi, T., Tomita, Y., and Kshu, Y., AFM observation of microscopic behavior of glassy polymer undr macroscopic tension, Trans. JSME, 1998, **64A** ,758-764.(in Japanese)
12. G'Sell, C. and Gopez, A. J., Plastic banding in glassy polycarbonate under plane simple shear. J. Mat. Sci. 1985, **20**, 3462-3478.
13. Harward, R. N. and Thackray, G., The use of a mathematical model to describe isothermal stress-strain curves in glassy thermoplastics. Proc. R. Soc. Lond., 1968, **A302**, 453-472.
14. Tomita, Y. and Adachi, Nonaffine network model for glassy polymer and prediction of instability propagation, T., De Borst, R and Van der Giessen, E., eds. Proc. IUTAM Symposium on Materials Instabilities, 1998, Wiley & Sons Ltd., 303-321.
15. Katagiri, K. 1997. Private Communication.
16.Hill, R., A general theory of uniqueness and stability in elastic-plastic solids. J. Mech. Phys. Solids, 1958, **10**, 236-249.
17.Kitagawa,H, Seguchi, Y. and Tomita, Y., An incremental theory of large strain and large displacement problems and its finite element application. Ing. Arch., 1972, **41**. 213-224.
18.Tomita, Y, Computational Elasto-plasticity, Yokendo, Tokyo,1990 (in Japanese)
19. Tomita, Y. and Hayashi, K., Thermo-elasto-viscoplastic deformation of polymeric bars under tension, Int. J. Solids Structs, 1993, **30**, 225-235.
20. Tomita, Y., Adachi, T., and Park, S. S., Computational simulation of the three-dimensional neck propagation in polymeric specimen under tension and hybrid identification of constitutive equation. Int. J. Mech. Sci., 1997, **39**, 913-923.
21. Wu, P. D. and Van der Giessen, E., On neck propagation in amorphous glassy polymers under plane strain tension. Int. J. Plast., 1995, **11**, 211-235

Figure Captions

Figure 1. Deformation behavior of glassy polymer under tension. (a) PC specimen profile, (b) nominal stress and elongation relation with deformed profile of specimen and (c) true stress and logarithmic strain relation.

Figure 2. AFM images of the surface of a PC specimen in undeformed sate and under tension in the five different regions a to e as indicated in the inset. The coordinates x, y and $\xi = x / B_0, \eta = y / B_0$ have the origin at the necking center. $a(\xi = 0.1.\eta = 0.71)$, $b(0.1,0.50)$, $c(0.1,0.12)$, $d(0.1,-0.34)$, $e(0.1,-0.76)$

Figure 3 Direction of plastic stretch θ_p and aligned microfibril structure θ_f versus shear strain ε_{xy}. W_0 to W_5 indicate the estimation points of θ_p and θ_f; $W_0(\xi = 0, \eta = 0)$, $W_1(1/12,0)$, $W_2(1/6,0)$, $W_3(1/4,0)$, $W_4(1/3,0)$, $W_5(5/12,0)$. θ_p and θ_f show the standard deviation for data numbers $n = 9$ and 4, respectively.

Figure 4. Hierarchy in the structure of polymeric materials: (a) segment, (b) single chain, (c) molecular chain network and (d) polymeric materials.

Figure 5 Computational models and boundary conditions. (a) Plane strain case. $L_0 / H_0 = 4$, $\varsigma = 0.005$, $H_0 = 3mm$, $\dot{\varepsilon}_0 = 2/\sqrt{3}(\dot{u} / L_0)$, (b) Three dimensional cases. $L_0 / H_0 = 20/3$, $t_0 / H_0 = 1/2$, $\dot{\varepsilon}_0 = \dot{u} / L_0$. Initial imperfection for both cases is $H_0(1-\varsigma)(|x_3| \le L_0 / 4)$.

Figure 6 (a) Nominal stress σ_n / s_0 and lateral contraction ratios $1 - H / H_0$, and $1 - t / t_0$ versus elongation u / L_0. (b) Deformed profiles and representative strain rate $\dot{\varepsilon}^p / \dot{\varepsilon}_0$ distributions at a to f as indicated in (a).

Figure 7 (a) Nominal stress σ_0 / s_0 and lateral contraction v / W_0 versus elongation u / L_0 for different deformation rates; $\dot{U} = \dot{\varepsilon}_0 / \dot{\varepsilon}_r, \dot{\varepsilon}_0 = 2\dot{u} / (\sqrt{3}L_0)$, $\dot{\varepsilon}_r = 10^{-4} / s$, $T_0 = 296K$. (b) Representative strain rate $\dot{\varepsilon}^p / \dot{\varepsilon}_0$, change of temperature $\Delta T / T_0$, distortion ξ and change in number of entangled points $\Delta m / m_0$ for $\dot{U} = 1, 10^2$ and 10^4.

Figure 8. (a) Nominal stress σ_n / s_0 versus elongation u / L with $PDR = 1.4$ and $\theta = 0 - 90^\circ$ and (b) distributions of representative strain rate $\dot{\varepsilon}^p / \dot{\varepsilon}_0$ on the blocks with $PDR = 1.4$ and various θ at $u / L = 0.05, 0.15$.

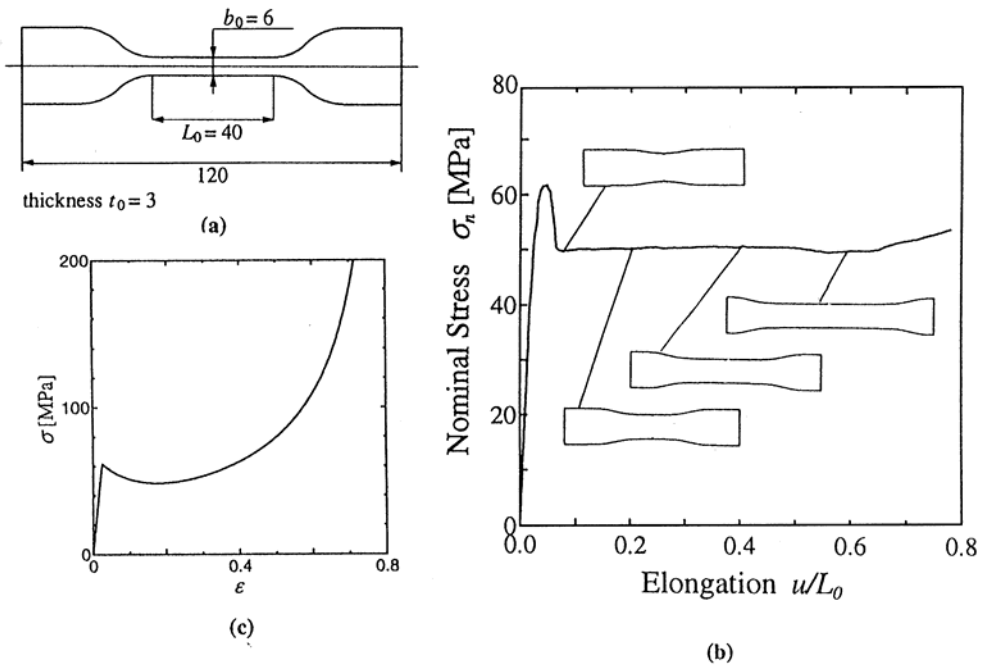

Figure 1.

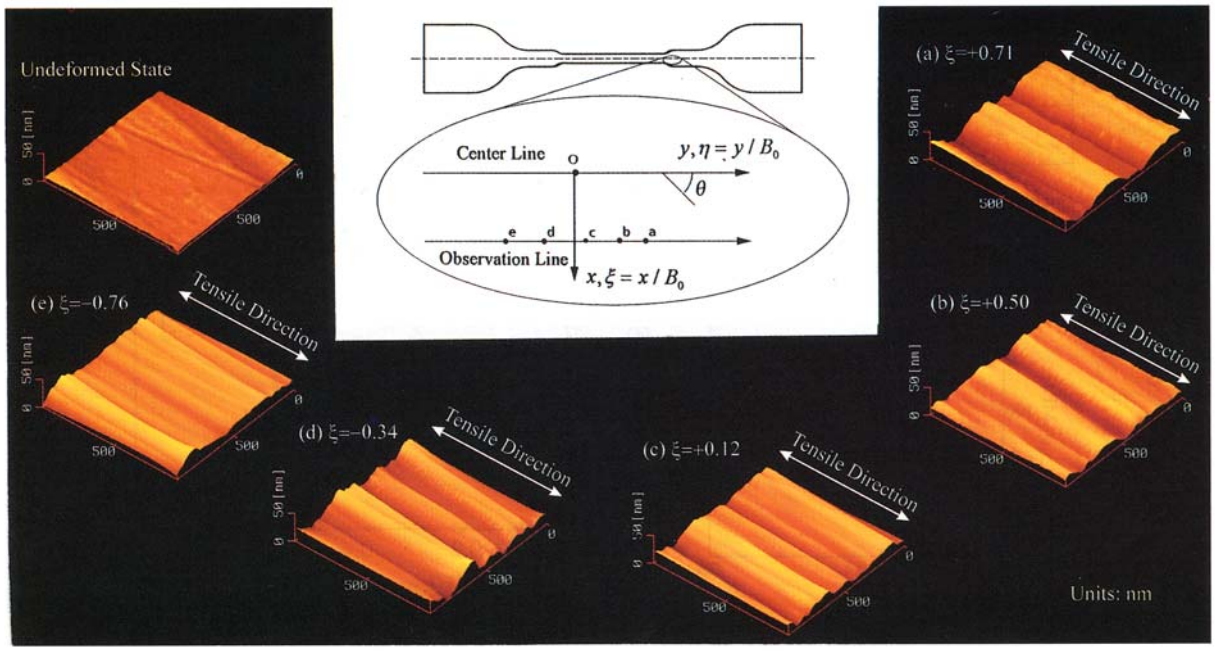

Figure 2.

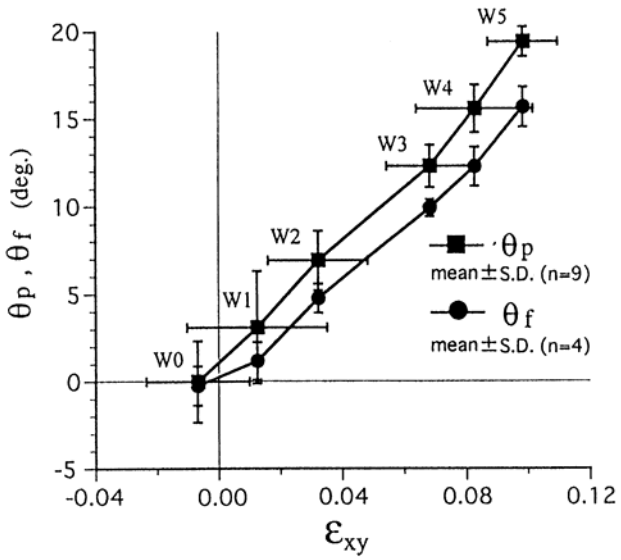

Figure 3.

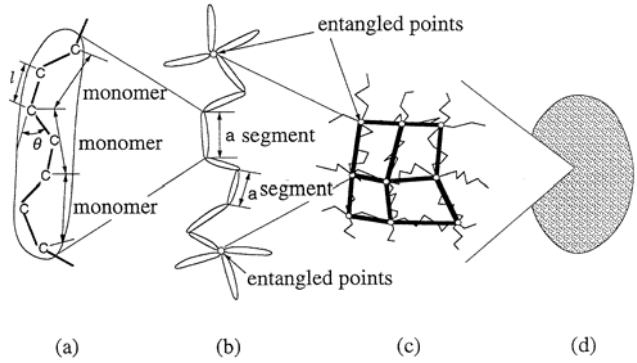

Figure 4.

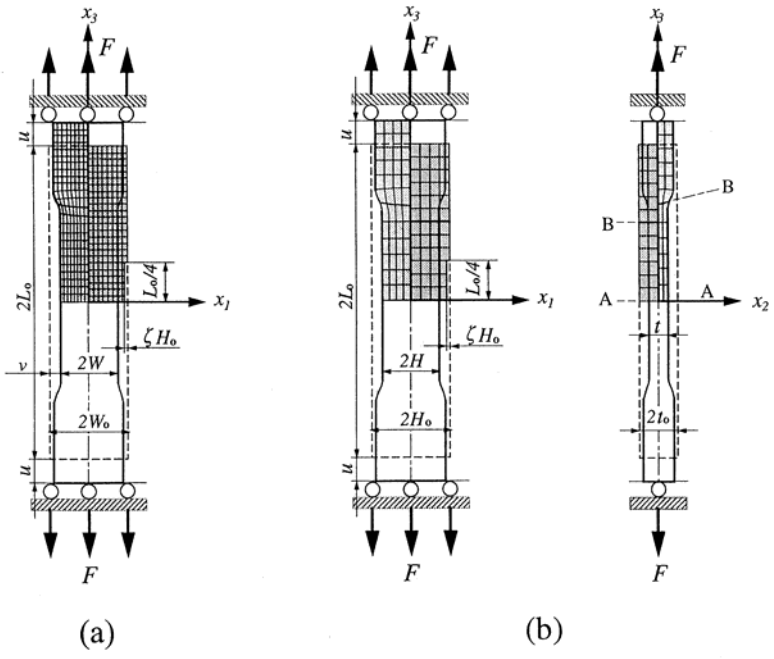

Figure 5.

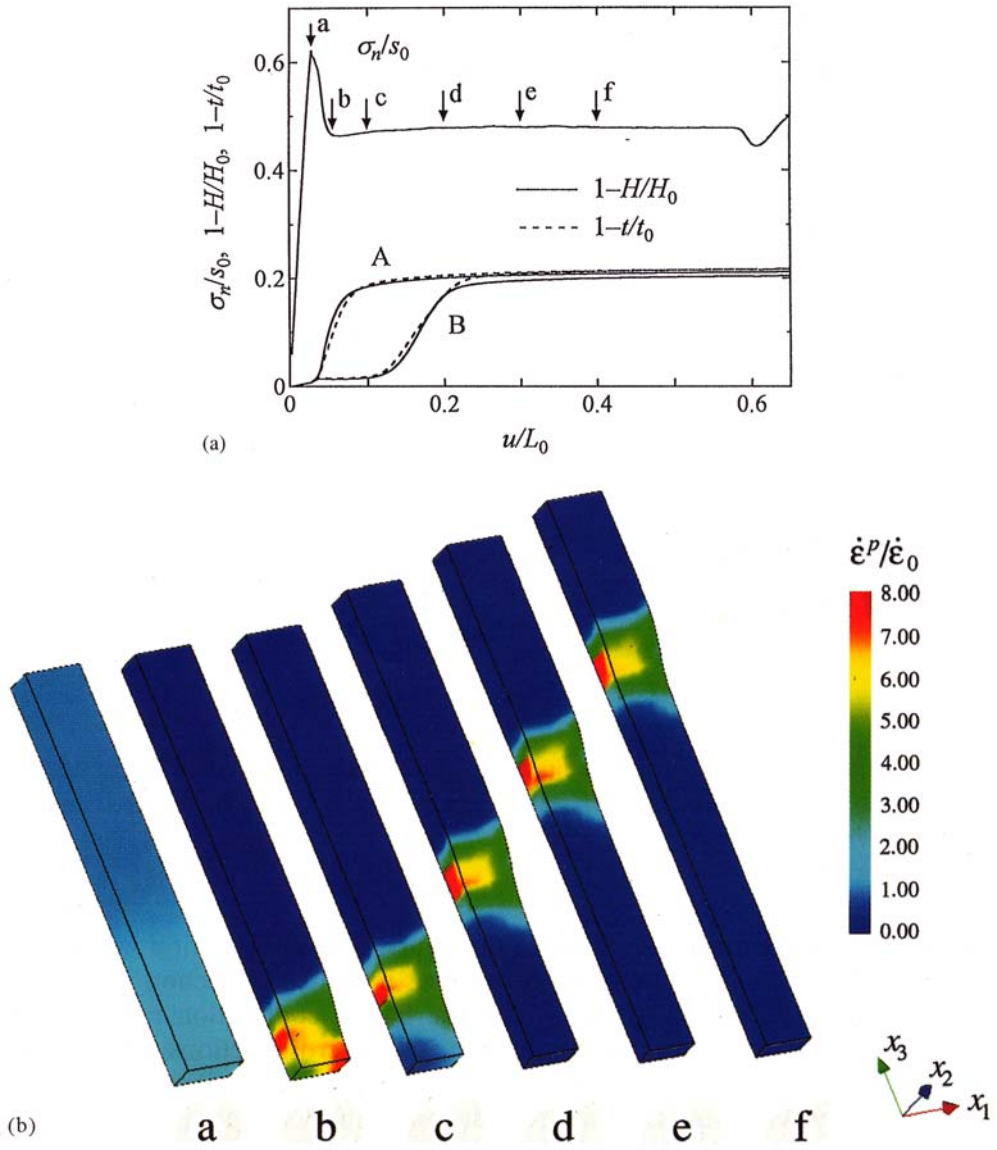
a
b
c
d
e
f
σ_n/s_0
$1-H/H_0$
$1-t/t_0$
A
B
σ_n/s_0, $1-H/H_0$, $1-t/t_0$
u/L_0
0
0.2
0.4
0.6
(a)
$\dot{\varepsilon}^p/\dot{\varepsilon}_0$
8.00
7.00
6.00
5.00
4.00
3.00
2.00
1.00
0.00
x_3
x_2
x_1
(b)
a
b
c
d
e
f

Figure 6.

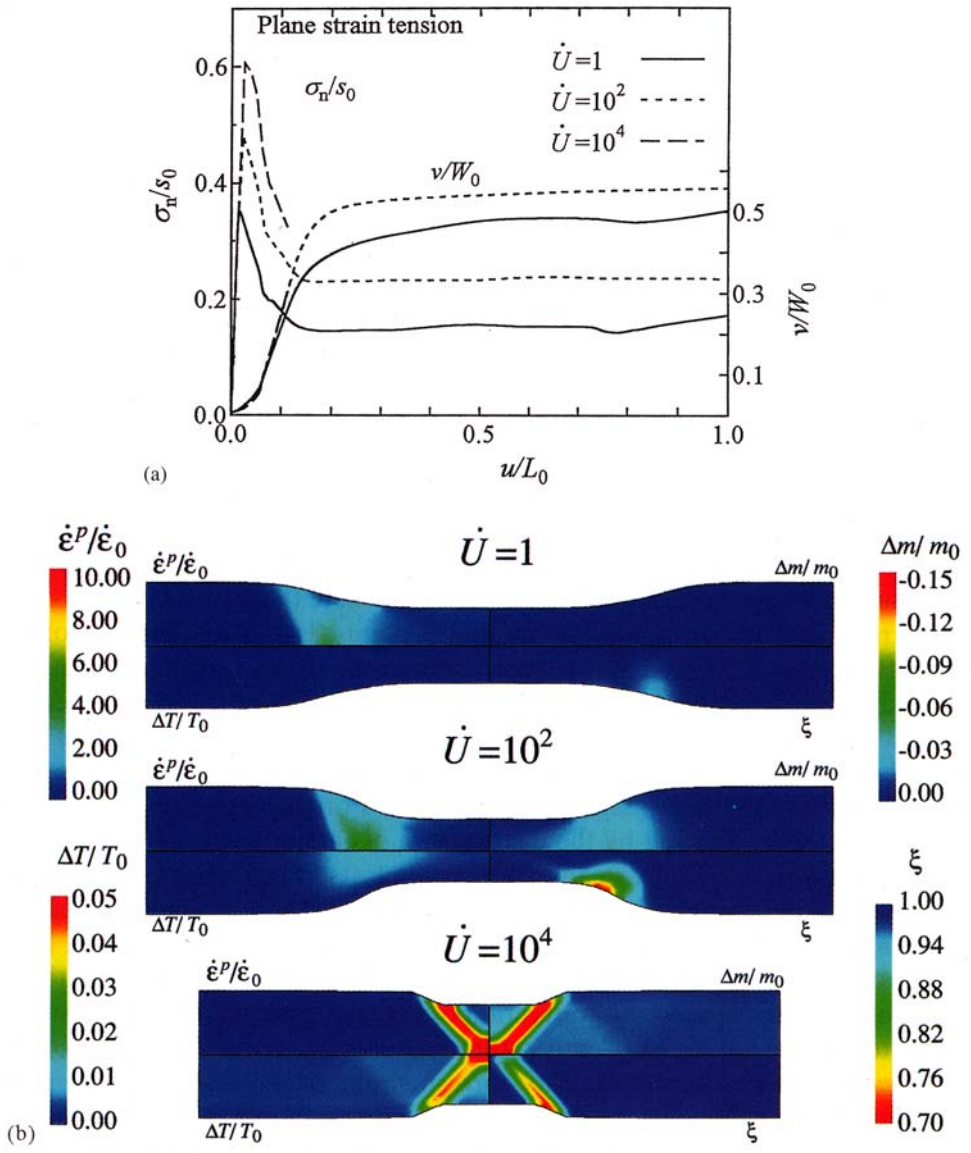
Plane strain tension
$\dot{U}$=1
$\dot{U}$=10^2
$\dot{U}$=10^4
σ_n/s_0
v/W_0
u/L_0
(a)
$\dot{\varepsilon}^p/\dot{\varepsilon}_0$
$\Delta T/T_0$
$\Delta m/m_0$
ξ
$\dot{U}$=1
$\dot{U}$=10^2
$\dot{U}$=10^4
(b)

Figure 7.

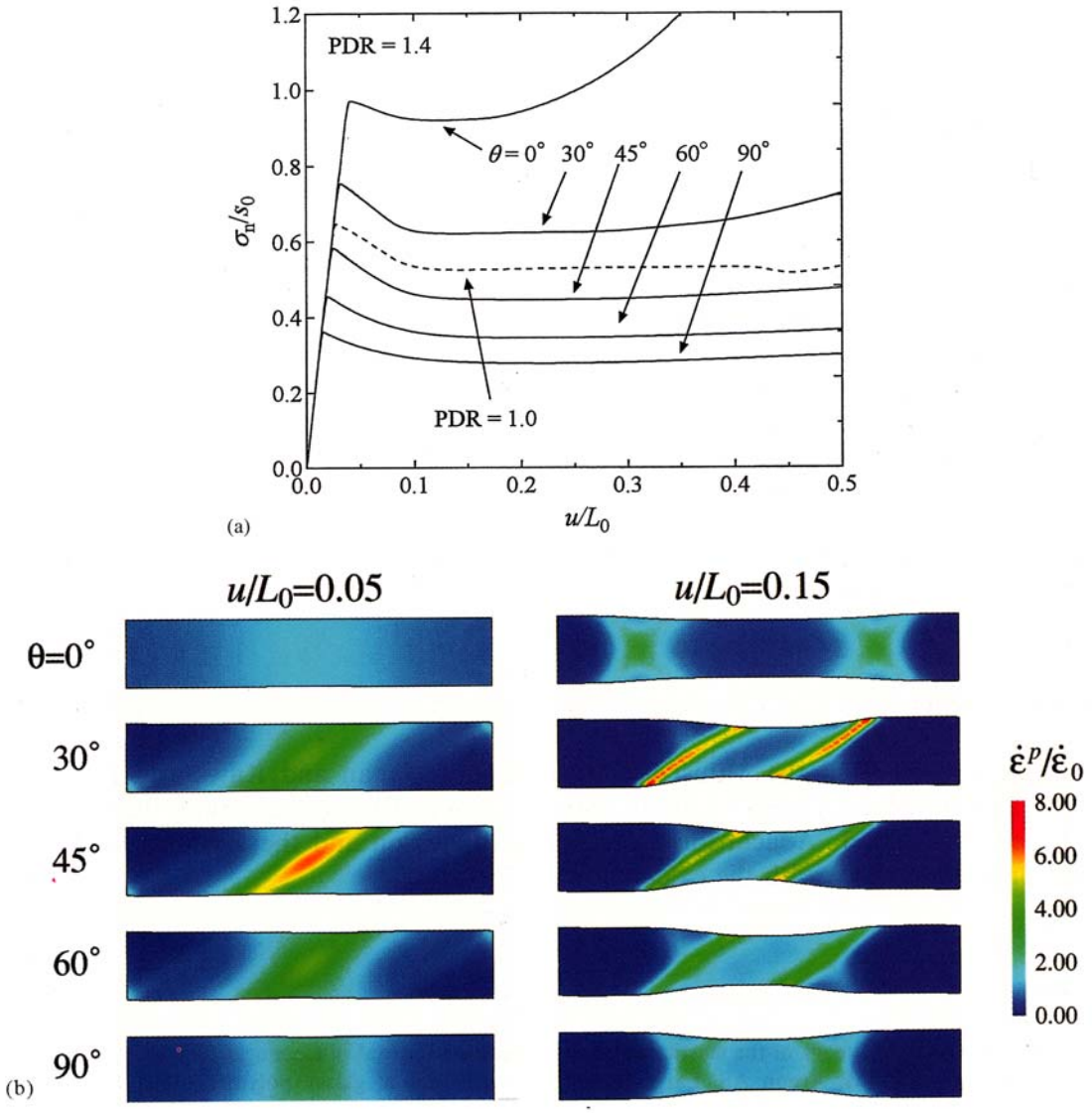
PDR = 1.4
θ = 0° 30° 45° 60° 90°
PDR = 1.0
σn/s0
u/L0
(a)
u/L0=0.05
u/L0=0.15
θ=0°
30°
45°
60°
90°
(b)
ε̇p/ε̇0
8.00
6.00
4.00
2.00
0.00

Figure 8.